Can we estimate precipitation rate during snowfall using a scanning terrestrial LiDAR?

Edward H. Bair[1,2]*, Robert E. Davis[1], David C. Finnegan[1], Adam L. LeWinter[1], Ethan Guttmann[3], and Jeff Dozier[4]
[1] US Army Corps of Engineers Cold Regions Research and Engineering Laboratory, Hanover, NH, USA
[2] Earth Research Institute, University of California, Santa Barbara, CA, USA
[3] National Center for Atmospheric Research, Boulder, CO, USA
[4] Bren School of Environmental Science & Management, University of California, Santa Barbara, CA, USA

ABSRACT: Accurate snowfall measurements in windy areas have proven difficult. To examine a new approach, we have installed an automatic scanning terrestrial LiDAR at Mammoth Mountain, CA. With this LiDAR, we have demonstrated effective snow depth mapping over a small study area of several hundred m^2. The LiDAR also produces dense point clouds by detecting falling and blowing hydrometeors during storms. Cumulative raw counts of airborne detections from the LiDAR show excellent agreement (R^2 > 0.90) with automated and manual snow water equivalent measurements, suggesting that LiDAR observations have the potential to directly estimate precipitation rate. Thus, we suggest LiDAR scanners offer advantages over precipitation radars, which could lead to more accurate precipitation rate estimates. For instance, uncertainties in mass-diameter/mass-fallspeed relationships used in precipitation radar, combined with low reflectivity of snow in the microwave spectrum, produce errors of up to 3X in snowfall rates measured by radar. Since snow has more backscatter in the near-infrared wavelengths used by LiDAR compared to the wavelengths used by radar, and the LiDAR detects individual hydrometeors, our approach has more potential for directly estimating precipitation rate. A key uncertainty is hydrometeor mass. At our study site, we have also installed a Multi Angle Snowflake Camera (MASC) to measure size, fallspeed, and mass of individual hydrometeors. By combining simultaneous MASC and LiDAR measurements, we estimate precipitation concentration and rate.

KEYWORDS: precipitation, lidar, mass flux

1 INTRODUCTION

Accurate and frequent measurement of snow water equivalent (SWE) is a longstanding problem due to wind and other biases. Manual measurement techniques, such as weighing snow cores or melting snow collected in a cylinder, are accurate, but are tedious and have poor temporal resolution (i.e. 1x/day). These manual measurements also only account for SWE on the ground. Post-depositional processes such as: melt, redistribution by wind, and sublimation cause differences between measurements of falling snow and snow on the ground. Automated instruments can measure falling snow frequently, but suffer from a variety of biases. In windy areas, automated measurements are especially difficult, since wind is the single largest contributor to under catch. For the most commonly used precipitation gauges in the world, catch ratios (the ratio of measured to actual precipitation) decrease nearly linearly with wind speed. For winds of 6 m sec^{-1} and snow at -2 ºC, one of the more accurate shielded gauges, the Canadian Nipher, has a catch ratio of 0.76 (Goodison et al. 1998). Other shielded gauges have catch ratios < 0.5 (Rasmussen et al. 2011).

Radar reflectivity is often used by meteorologists to measure precipitation rates. Estimating precipitation rate from radar returns requires assumptions about the size of the hydrometeors. For rainfall, the diameter of the drops D over the volume sampled V can be used to predict radar reflectivity Z (Marshall et al. 1947):

$$Z = \frac{\Sigma D^6}{V} \quad (1)$$

With rainfall, there is a definite relationship between hydrometeor mass m and diameter D:

$$m = \frac{\pi}{6}\rho D^3 \quad (2)$$

where ρ is the density of water. Thus, radar reflectivity is a good predictor of precipitation rate R using a power law:

* Corresponding author address: Edward H. Bair, Earth Research Institute, University of California, Santa Barbara CA 93106-5131, USA, email: nbair@eri.ucsb.edu

$$R = aZ^b \quad (3)$$

with *a* and *b* estimated empirically. For snow, there is large scatter in the mass-diameter relationship. A power law is usually used:

$$m = bD^c \quad (4)$$

,but the coefficients vary widely with *b*=0.001-0.070 and *c*=2.0-2.5 (Heymsfield et al. 2002; Matrosov et al. 2009). As a result, radar reflectivity is a poor predictor of precipitation rate during snowfall.

Another problem with using radar to measure snowfall rate is that snow, unlike rain, is weakly reflective in the microwave spectrum. For commonly used precipitation radars in the US, light to heavy rain shows reflectivities of 20-65 dBZ, while light to heavy snow has reflectivities of 20-35 dBZ, with reflectivities < 20 dBZ for snowfalls of a single crystal habit (Matrosov et al. 2009).

To examine a new approach, we have installed an automatic scanning terrestrial lidar at Mammoth Mountain, CA. This instrument can effectively map snow depth over a small study area of several hundred m^2. This LiDAR also produces dense point clouds by detecting falling and blowing hydrometeors during storms. Using measurements from automated precipitation gauges and manual SWE cores taken nearby daily, we examine empirical relationships between the in-air lidar detections and precipitation rate. From these empirical relationships, we introduce a sampling theory for the lidar detections.

2 METHODS

2.1 Instrument

The lidar used is a Riegl LMS-Z390i. The instrument uses an infrared laser with wavelength 1.55 µm. The scanner is capable of 360º azimuthal and 80º elevational coverage at 0.09º angular increments. The beam diameter is 6.5 mm at the aperture, with 0.3 mrad divergence. The lidar is enclosed in a custom-made glass case (Figure 1) and automatically scans every hour or every 15 min. The enclosure is mounted on a steel platform, approximately 7 m above snow-free ground.

Figure 1 Lidar and enclosure at CUES

2.2 Site

The lidar is installed at the Cold Regions Research and Engineering Laboratory/University of California – Santa Barbara Energy balance site (CUES, www.snow.ucsb.edu/cues/). The site is located at 2940 m on Mammoth Mountain, CA.

The vegetation at CUES is sub-alpine, consisting of sparsely spaced conifers. CUES has significant wind exposure, averaging 4 m sec^{-1} from the southwest.

2.3 Data processing

Because of an internal range gate, the lidar does not record detections closer than about 2 m. Also, to eliminate artifacts caused by seams in the glass enclosure and to ensure that only in-air hydrometeors were sampled, a small sample volume within each scan was used. The resulting sample volume was approximately 10 x 10º at 3-4 m distance, or 0.37 m^3. The sample volume location was directly in front of the scanner, about level with the ground, but at least 3 m above the snow surface (Figure 2).

The lidar produces files in a proprietary format (3dd), which we converted to an ASCII format containing Cartesian coordinates (X,Y,Z) and relative intensities (0-1) for each detection. From the coordinates, we recorded the number of detections in the sample volume and the associated scan time.

2.4 Ancillary precipitation measurements

Precipitation measurements are available from several sources. At CUES, there is a Lufft WS-600 precipitation sensor that uses at 24 Ghz Doppler radar. The nearest manual SWE measurements come from the Mammoth

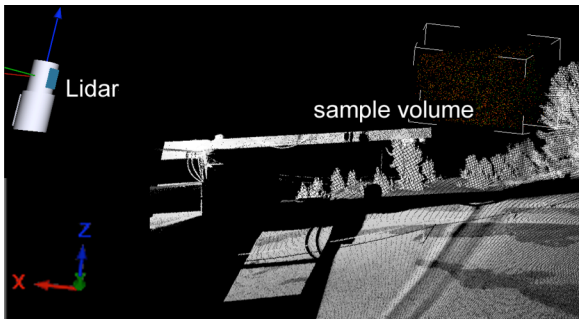

Figure 2 Overlay of clear weather lidar scan with precipitation in sample volume

Mountain Ski Patrol Sesame snow plot at 2,743 m, also on Mammoth Mountain. Wind exposure here is slightly less; winds average 3.3 m sec^{-1}. The Sesame site also has two different shielded automated precipitation gauges and another WS-600.

Based on comparisons with manual SWE measurements at the Sesame site, we found that both precipitation cans consistently under caught precipitation, with catch ratios of 0.20 or worse. Wind effects and clogging from ice build-up were the main causes. At both sites, the WS600 underestimated precipitation by similar amounts.

At the nearby Mammoth Pass, el. 2835 m, the US Bureau of Reclamation operates a precipitation gauge in a more wind sheltered area. Comparisons with manual SWE measurements at Sesame show a less severe under catch bias (catch ratios around 0.80). Thus, because of under catch issues, we decided the daily manual SWE measurements were the only reliable precipitation measurements from similar sites nearby.

We also attempted to correlate lidar counts with snow depth from ultrasonic depth pingers at CUES, but on going snow settlement during storms made it impossible to separate the effects of settlement from those of accumulation.

2.5 Sampling issues:

From Mar 2011 to Feb 2012, the LiDAR scanned hourly. On 13 Feb 2012, the scan frequency was increased to 15 min to obtain more accurate precipitation rate estimates.

3 RESULTS

3.1 Empirical correlations

Hourly (Figure 3) and 15 min scans (Figure 4), summed daily, both followed manually weighed SWE from Sesame. The 15 min scans had stronger correlation (r=0.73) than the hourly data (r=0.58), which was expected. The day with the highest manually weighed SWE amount (17 Mar 2012, 145 mm SWE) had the highest sums of lidar counts for both sampling frequencies, but the rank of other days did not match. For instance, the day with the 2nd most manually weighed precipitation during the 15 min scans (14 Apr 2012, 77 mm SWE) ranked 16th in the 15 min lidar sums.

4 SAMPLING THEORY AND DISCUSSION

To better understand what the lidar records during precipitation, we developed a sampling theory.

4.1 Beam coverage

Because of spacing between laser beams, they overlap at short distances and leave gaps at longer distances. To model beam coverage, we computed the beam area A as:

$$A(d) = \pi {r_f}^2 \qquad (5)$$

where r_f is the radius of the beam footprint at distance d. The beam radius was computed using right triangle geometry (Figure 5):

$$r_f(d) = (d + d_i)\tan\frac{\delta}{2} \qquad (6)$$

where δ is the divergence angle, 3 x 10^{-3} rad, and d_i is the internal distance; that is distance from a hypothetical origin to the laser aperture, such that:

$$d_i = \frac{w}{2}\cot\frac{\delta}{2} \qquad (7)$$

where w is the width of the laser beam at the aperture, 6.5 x 10^{-3} m. The beam area was then converted to a solid angle Ω_b,

$$\Omega_b(d) = \frac{A(d)}{d^2} \qquad (8)$$

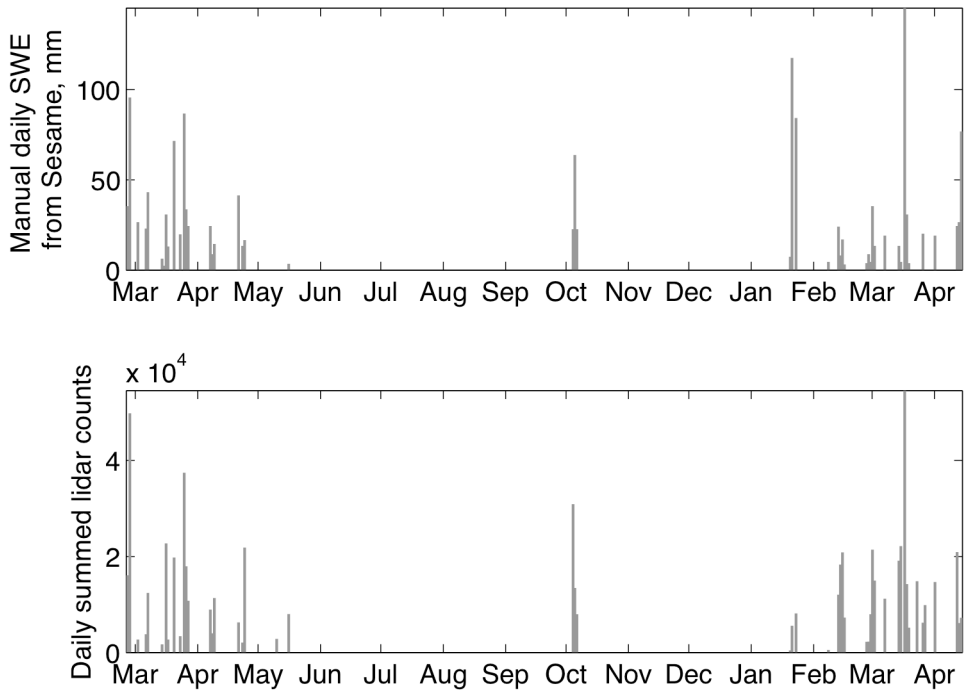

Figure 3 Daily manual SWE and summed lidar counts, hourly. The sums are from hourly lidar scans from March 2011-April 2012. The correlation coefficient *r*=0.58.

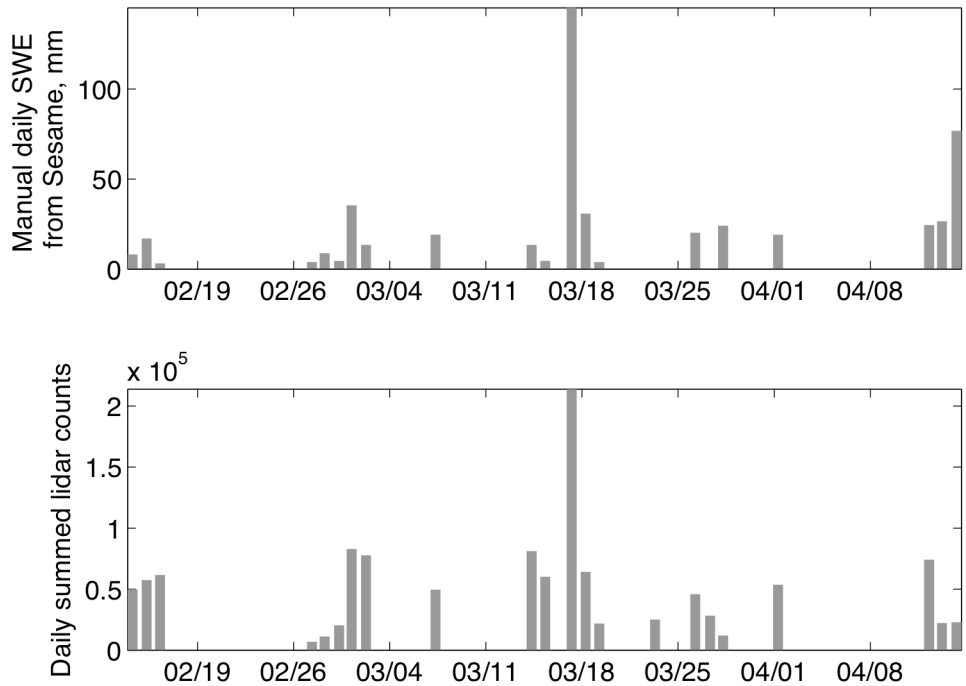

Figure 4 Daily manual SWE and summed lidar counts, 15 min. The sums are from 15 min lidar scans from Feb-April 2012. The correlation coefficient *r*=0.73.

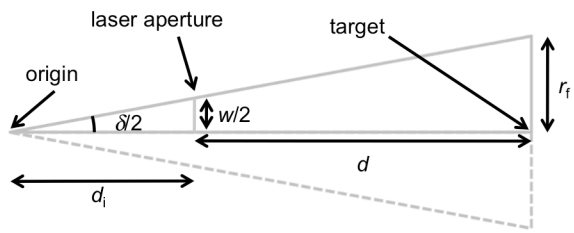

Figure 5 Beam geometry

and compared to the solid angle Ω_s

$$\Omega_s = 2\delta \sin\left(\frac{\delta}{2}\right) \tag{9}$$

subtending the square bounded by $\pm\delta/2$ on each side. The ratio of Ω_b to Ω_s gives an efficiency E

$$E(d) = \frac{\Omega_b(d)}{\Omega_s} \tag{10}$$

that represents coverage by the beam at distance d. Efficiency decreases as a power law with distance (Figure 6). At 3-4 m, the distance for the sample volume, the lidar oversamples; efficiencies range from 1.9 to 1.1. Knowing that the lidar oversamples at the distances chosen, we can develop an adjustment factor α,

$$\alpha n = q \tag{11}$$

This factor adjusts the concentration of hydrometeors detected n to the actual concentration of hydrometeors q. It should equal the reciprocal of E multiplied by β, the ratio of lidar pulses transmitted to those received:

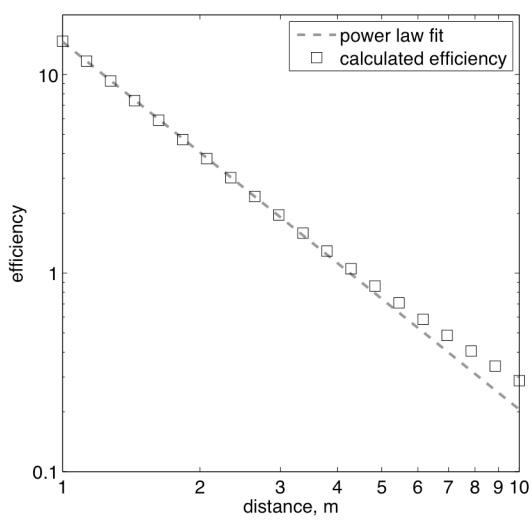

Figure 6 Lidar efficiency vs. distance to target. The power law fit is $y=ax^b$, with a=14.63 and b=-1.85 (RMSE=0.066).

$$\alpha = \frac{1}{\beta E} \tag{12}$$

Mass flux j is:

$$qmv = j \tag{13}$$

where m is the mass of each hydrometeor, kg, and v is fallspeed, m sec^{-1}. To convert j into mm hr^{-1} to compare with the Sesame average precipitation rate measurements $\bar{R}$:

$$j = \frac{\bar{R}}{3600\,\mathrm{mm\ hr^{-1}\,kg^{-1}\,m^2\,sec}} \tag{14}$$

since 1 mm water per m^{-2} weighs 1 kg. Combining Eqs. 11, 13, and 14; and solving for α yields:

$$\alpha = \frac{\bar{R}}{nmv} \times \frac{1}{3600\,\mathrm{mm\ hr^{-1}\,kg^{-1}\,m^2\,sec}} \tag{15}$$

We analyze a specific day of precipitation, 26 Mar 2012, since that is one of the few days when the MASC was working where we have mass and fallspeed measurements. Over 25 hr, 20 mm of SWE was manually weighed, corresponding to $\bar{R}$=0.8 mm hr^{-1}. Over the same period, there were 45,949 lidar detections (taken every 15 min) in a sample volume of 0.37 m^{-3}. Thus, for each scan, the average concentration n=1,241 m^{-3}. Using median values from measurements taken by the Multi-Angle Snowflake Camera (MASC, Garrett et al. 2012) installed at CUES, m=0.4 mg and v=0.6 m sec^{-1} (Figure 7). Note there is no relationship between mass and fallspeed in the MASC measurements, as has been suggested in other studies (e.g. Mitchell et al. 1990). Using these values in Eq. (15) gives α=0.75. Solving for β in Eq. (12) gives 0.89, using a mean efficiency value of E=1.5. This value for β indicates that 89% of the hydrometeors in the sample volume were detected. This is feasible, given that snow is forward scattering at 1.55 μm, but the reflectance is dependent on snowfall rate. Absorption at 1.55 μm is negligible, since the complex refractive index of ice at 1.55 μm is 10^{-3} (Wiscombe and Warren 1980). Reflectance values similar to β have been measured in falling snow using forward scatter meters (Koh 1987), which suggests that 0.89 is a reasonable value for β.

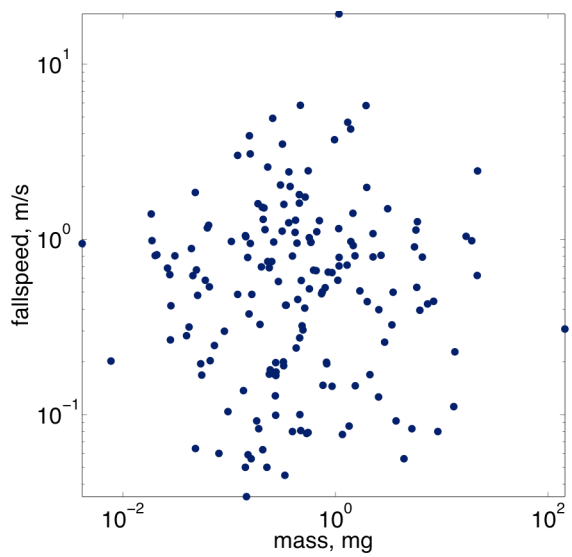

Figure 7 Mass and fallspeed of solid precipitation measured by the Multi-angle Snowflake Camera (MASC) from 25 to 26 Mar 2012.

The MASC shows wide variation in measured values of *m* and *v*. For instance, using 25th and 75th percentiles of measurements taken by the MASC, m=0.2-1.1 mg and v=0.2-1.1 m sec^{-1}. Those percentiles give a wide range for the adjustment factor, α=0.15-4.48, highlighting its sensitivity to mass and fallspeed.

Values in the literature show similar variation and indicate the MASC mass estimates are too large. Ranges reported are m=0.002 to 0.100 mg and v=0.5-1.2 m sec^{-1}, depending on the crystal size, habit, and amount of rime (Mellor 1966; Gunn 1967; Mitchell et al. 1990). Using these smaller mass values would give values for the adjustment factor α that are up to two orders of magnitude larger. Such high values for α would indicate that we are not detecting nearly as many hydrometeors as we think (β << 0.89). Yet given the wide range and experimental difficulties in measuring hydrometeor mass, it is unclear if our sampling theory or measurements are flawed. In the past, studies have struggled with mass measurements of snowflakes, especially the larger ones.

It should be stated that the MASC does not directly measure mass; it uses images of snowflakes and image processing functions to estimate the amount of ice in each snowflake. Snowflakes with high dendricity (e.g. stellars) will likely have mass estimates that are too high, while rimed snowflakes with less dendricity should have more accurate mass estimates.

5 CONCLUSION

We have shown that, in addition to snow depth mapping (i.e. Deems et al. 2006; Prokop 2008), lidar can also be used for snow mass flux estimates.

We found good empirical agreement between lidar counts in a sample volume, summed over one day, and manually weighed SWE from a nearby site.

Currently, we lack precise hydrometeor mass estimates that are essential for validating our approach of measuring mass flux. For mass measurements, we are relying on a prototype instrument, the MASC, that requires constant maintenance and repair. Also, its mass measurements have not been independently verified. As we improve the MASC and validate its measurements, we will obtain reliable estimates for hydrometeor mass, which will improve our mass flux estimates.

Another goal is to co-locate the lidar with a reliable precipitation gauge, which would likely involve moving it to a sheltered area that is more suitable for precipitation gauge measurements. This would give a reliable ground truth for precipitation rate to compare with lidar counts.

6 REFERENCES

Deems, J. S., S. R. Fassnacht, and K. J. Elder, 2006: Fractal distribution of snow depth from lidar data. *J. Hydrometeorol.*, **7,** 285-297.

Garrett, T., E. Bair, C. Fallgatter, K. Shkurko, R. Davis, and D. Howlett, 2012: The Multi-Angle Snowflake Camera. *Proceedings of the 2012 International Snow Science Workshop*.

Goodison, B., P. Y. T. Louie, and D. Yang, 1998: WMO Solid precipitation measurement intercomparison.

Gunn, K. L. S., 1967: The number flux of snow crystals at the ground. *Monthly Weather Review*, **95,** 921-924.

Heymsfield, A. J., and Coauthors, 2002: A General Approach for Deriving the Properties of Cirrus and Stratiform Ice Cloud Particles. *J.*

Atmos. Sci., **59,** 3-29, doi:10.1175/1520-0469(2002)059<0003:agafdt>2.0.co;2.

Koh, G., 1987: Extinction coefficient measurement in falling snow with a forward scatter meter, 13 pp.

Marshall, J. S., R. C. Langille, and W. M. K. Palmer, 1947: Measurement of rainfall by radar. *Journal of Meteorology*, **4,** 186-192, doi:10.1175/1520-0469(1947)004<0186:morbr>2.0.co;2.

Matrosov, S. Y., C. Campbell, D. Kingsmill, and E. Sukovich, 2009: Assessing Snowfall Rates from X-Band Radar Reflectivity Measurements. *J. Atmos. Ocean. Technol.*, **26,** 2324-2339, doi:10.1175/2009jtecha1238.1.

Mellor, M., 1966: Light scattering and particle aggregation in snow-storms. *Journal of Glaciolgy*, **6,** 237-248.

Mitchell, D., R. Zhang, and R. Pitter, 1990: Mass-dimensional relationships for ice particles and the influence of riming on snowfall rates. *Journal of Applied Meteorology*, **29,** 153-163.

Prokop, A., 2008: Assessing the applicability of terrestrial laser scanning for spatial snow depth measurements. *Cold Regions Science and Technology*, **54,** 155-163, doi:10.1016/j.coldregions.2008.07.002.

Rasmussen, R., and Coauthors, 2011: The NOAA/FAA/NCAR Winter Precipitation Test Bed: How Well Are We Measuring Snow? *Bulletin of the American Meteorological Society*, doi:10.1175/bams-d-11-00052.1.

Wiscombe, W. J., and S. G. Warren, 1980: A model for the spectral albedo of snow, I, Pure snow. *J. Atmos. Sci.*, **37,** 2712-2733, doi:10.1175/1520-0469(1980)037<2712:AMFTSA>2.0.CO;2.